Symbiosis-inspired de novo synthesis of ultrahigh MOF growth mixed matrix membranes for sustainable carbon capture

Shanshan He[a], Bin Zhu[a], Xu Jiang[b], Gang Han[c], Songwei Li[d], Cher Hon Lau[e], Yadong Wu[a], Yanqiu Zhang[a], and Lu Shao[a,1]

[a]MIIT (Ministry of Industry and Information Technology) Key Laboratory of Critical Materials Technology for New Energy Conversion and Storage, State Key Laboratory of Urban Water Resource and Environment, School of Chemistry and Chemical Engineering, Harbin Institute of Technology, Harbin 150001, China; [b]Singapore Membrane Technology Centre, Nanyang Environment and Water Research Institute, Nanyang Technological University 637141 Singapore, Singapore; [c]Department of Chemical Engineering, Massachusetts Institute of Technology, Cambridge, MA 02139; [d]Key Laboratory of Materials Processing and Mold, Ministry of Education, National Engineering Research Center for Advanced Polymer Processing Technology, Department of Chemical Engineering, Zhengzhou University, Zhengzhou 450002, China; and [e]School of Engineering, The University of Edinburgh, Edinburgh EH9 3JL, United Kingdom

Mixed matrix membranes (MMMs) are one of the most promising solutions for energy-efficient gas separation. However, conventional MMM synthesis methods inevitably lead to poor filler–polymer interfacial compatibility, filler agglomeration, and limited loading. Herein, inspired by symbiotic relationships in nature, we designed a universal bottom-up method for in situ nanosized metal organic framework (MOF) assembly within polymer matrices. Consequently, our method eliminating the traditional postsynthetic step significantly enhanced MOF dispersion, interfacial compatibility, and loading to an unprecedented 67.2 wt % in synthesized MMMs. Utilizing experimental techniques and complementary density functional theory (DFT) simulation, we validated that these enhancements synergistically ameliorated CO_2 solubility, which was significantly different from other works where MOF typically promoted gas diffusion. Our approach simultaneously improves CO_2 permeability and selectivity, and superior carbon capture performance is maintained even during long-term tests; the mechanical strength is retained even with ultrahigh MOF loadings. This symbiosis-inspired de novo strategy can potentially pave the way for next-generation MMMs that can fully exploit the unique characteristics of both MOFs and matrices.

gas separation | ZIF-8 | mixed matrix membrane | carbon capture | symbiosis-inspired synthesis

In recent years, global carbon emissions have increased rapidly, pushing atmospheric CO_2 levels to record levels that cause devastating climate change (1–4). Under such critical circumstances, highly efficient carbon capture technologies, which are estimated to be a global market of $6.13 billion by 2027, must be implemented to achieve carbon neutrality (5). Currently, membrane separation is expected to be one of the most promising techniques for CO_2 capture on a large scale due to its relatively low cost, low carbon footprint, continuous operation, easy accessibility, and energy efficiency (6–8), which are distinct advantages compared to traditional separation technologies such as pressure swing adsorption.

As an emerging membrane material, first developed by Budd et al. (9, 10), polymers of intrinsic microporosity (PIMs) with ladder-like structures have been widely studied for carbon capture. The contortion sites and absence of single bonds in the PIM backbone lead to irregular and kinked chain architecture without conformational flexibility, further causing interconnected micropores and high specific surface area which endow PIMs with ultrahigh gas permeability (11, 12). PIM-1, the archetypal PIM with linear structure, is one of the most studied PIMs in gas separation because of its excellent solubility in common organic solvents (CH_2Cl_2, $CHCl_3$, etc.). However, gas

transportation in PIM-1 membranes is underpinned by the solution–diffusion mechanism, where high permeability is typically associated with low selectivity and vice versa (13, 14). In addition, inefficient packing of PIM-1 chains leads to a nonequilibrium state where molecular relaxation occurs over time, reaching an equilibrium state (15) and causing fractional free volume and permeability losses, i.e., physical aging (12, 16–18).

Incorporating nanofillers to fabricate PIM-1–based mixed matrix membranes (MMMs) is an effective strategy for simultaneously enhancing the gas separation performance and overcoming the physical aging of PIM-1 (19). Diverse nanomaterials have been deployed as fillers in MMMs, such as graphene oxide, carbon nanomaterials, zeolites, and metal oxides (20–23). Metal–organic frameworks (MOFs), constructed from metal ions/clusters and rigid organic ligands, are promising nanofillers with high specific surface areas and tunable pore sizes (24), which can effectively disrupt PIM-1 chain packing and create additional gas transportation channels to enhance membrane separation performance (19, 25–28). The fine dispersion of MOFs in polymer matrices, particularly at high filler contents, is crucial for achieving high-performance MMMs. The agglomeration of fillers and poor polymer–filler interfacial compatibility lead to interfacial defects and internal voids that notably decrease gas selectivity (29–31). To improve nanoparticle

Significance

The development of highly efficient carbon capture technology is the most crucial step for achieving the carbon neutrality target, which is estimated to have a global market value up to $6.13 billion by 2027. Advanced membranes, as efficient CO_2 separation strategies, significantly promote the development of clean energy and low-carbon technologies. Studies on next-generation mixed matrix membranes (MMMs) are highly expected to combine excellent workability and high gas separation performance capable of sustainable energy-efficient carbon capture.

dispersion and enhance interfacial compatibility, approaches such as designing polymer-embedded MOFs (32), MOF surface functionalization (33–35), and MOF morphology regulation (36) have been deployed. In these methods, MMMs are normally prepared in at least two steps, where MOFs are first synthesized and then incorporated into a polymer matrix. The main limitation of such approaches is that upon postsynthetic drying, nanoparticles are extremely difficult to sufficiently redisperse in solvents. This is also why defect-free MMMs with high MOF loadings are rarely obtained, limiting the utilization of the intrinsic excellent gas adsorption and separation performances of MOFs. Fabricating MMMs with high MOF content remains highly challenging, especially based on highly permeable polymers such as PIM-1.

In nature, rhizobium, a class of bacteria, invades plant roots and stimulates specific cells in the cortex and pericycle of the root. This causes intense cell growth and local swelling of the root, which forms nodules for harmonious integrated symbiosis. Inspired by this natural process, we developed a bottom-up strategy for the in situ growth of ZIF-8 in highly permeable PIM-1 using a screened chloroform/water mixed solvent. We then constructed defect-free MMMs with ultrahigh ZIF-8 loading for gas separation. During the synthesis, the aqueous ZIF-8 precursor solution was mixed with the PIM-1/CHCl$_3$ solution under vigorous stirring to form an oil–water mixture, which created a homogeneous distribution of the grown ZIF-8 nanoparticles in PIM-1. By adjusting the precursor content, ultrahigh MOF loading can be easily achieved. The entanglement of PIM-1 chains and the interactions between uncoordinated imidazole groups of ZIF-8 and -CN groups of PIM-1 ensured simultaneous precipitation in MeOH to form the floccules containing well-mixed PIM-1 and ZIF-8, maintaining excellent interfacial compatibility. We investigated the synthesized MMMs with ultrahigh MOF content for gas separation and characterized the mechanisms underpinning their excellent gas separation performance by experiment and simulations. The universality of our symbiosis-inspired synthesis strategy was further demonstrated using different aqueous-synthesized MOFs (ZIF-7 and ZIF-67) and glassy polymer matrices (Matrimid).

Results and Discussion

In Situ Preparation of ZIF-8/PIM-1 MMMs in CHCl$_3$/Water Mixture.
Inspired by the winding structure of plant roots and the process of rhizobium-inducing nodules for integrated symbiosis, we developed a strategy for in situ MOF growth in a matrix of the archetypal PIM, PIM-1, to fabricate MMMs with ultrahigh MOF content for fully exploiting the merits of both MOFs and matrices. As illustrated in Scheme 1, the ZIF-8 precursors, Zn(NO$_3$)$_2$·6H$_2$O and dimethylimidazole (Hmim), were first dissolved in water and mixed with the PIM-1/CHCl$_3$ solution with vigorous stirring to form a uniform oil–water mixture. ZIF-8 nanoparticles crystallized gradually in the aqueous phase, which in situ mingled with PIM-1 polymer and dispersed evenly. Here water is present as a noncontinuous phase and is finely dispersed within the oily (CHCl$_3$) phase. The dispersion phase provides numerous microenvironments for ZIF-8 to grow gradually and slowly in water, while PIM-1 remains fully dissolved in the CHCl$_3$ phase. Moreover, the insufficient contact between the precursors retarded the ZIF-8 nucleation rate, reducing the average size of ZIF-8 nanoparticles by 50%, in comparison with ~200-nm ZIF-8 particles that were synthesized in a single water phase (*SI Appendix*, Fig. S4). The smaller particles effectively reduce particle agglomeration and improve the interfacial compatibility (36). Meanwhile, the uncoordinated imidazole groups on the surface of ZIF-8 nanoparticles interact with the nitrile groups of PIM-1, forming defect-free matrix–filler interfaces with good compatibility. The mixture was precipitated in pure
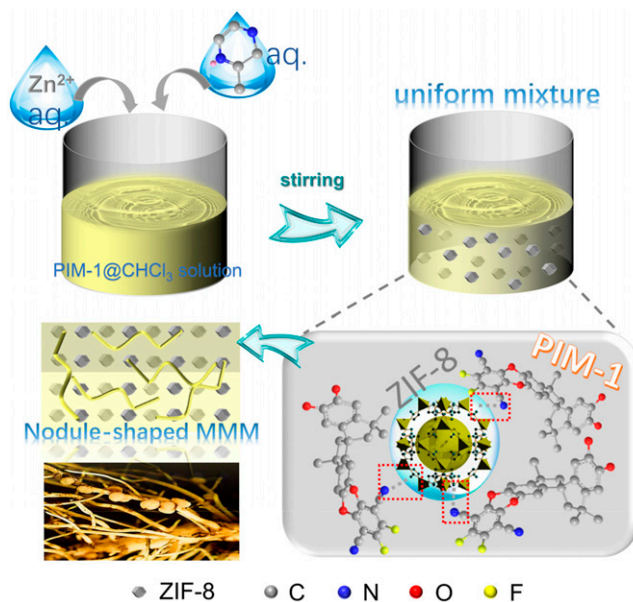
Scheme 1. Schematic illustrations of the preparation of ZIF-8/PIM-1 hybrid via the symbiosis-inspired in situ growth approach, where gray rhombic dodecahedron represents the ZIF-8 nanoparticles. PIM-1 and dimethylimidazole are represented via the molecular ball and stick model, where gray represents the C atom, red represents the O atom, blue represents the N atom, and yellow represents the F atom. The red frame highlights the (NH)$_{ZIF-8}$···(N)$_{PIM-1}$ interaction.

MeOH to obtain ZIF-8/PIM-1 floccules. PIM-1 intertwined ZIF-8 in the floccules mimicking symbiosis and prevented the separation of PIM-1 and ZIF-8. After washing, the symbiosis-inspired floccules were redissolved in CHCl$_3$ for fabricating ZIF-8/PIM-1 MMMs with ultrahigh ZIF-8 content via solvent evaporation. The membranes were named as x-ZIF-8/PIM-1, where x referred to the amount of Zn^{2+} with the unit of mmol.

To further confirm the excellent interface between PIM-1 and ZIF-8, a computational simulation that integrated density functional theory calculations and force field–based molecular dynamics (MD) simulations was performed to calculate the interactions of the NH terminal functions on the linkers at the surface of ZIF-8 with -CN, -OH, and -CH$_3$ groups of PIM-1, as illustrated in *SI Appendix*, Fig. S5 *A–C*. Furthermore, the radial distribution functions (RDFs) between different PIM-1-ZIF-8 atom pairs from the MD trajectories were calculated, giving the probability of molecules occurring at the distance (r). As presented in *SI Appendix*, Fig. S5 *D–F*, the series of RDFs indicated that the polymer chains were arranged to form a preferential interaction between the nitrogen atom of the cyano function and the -NH group of the ZIF-8, leading to a mean characteristic (NH)$_{ZIF-8}$-(CN)$_{PIM-1}$ distance of ~2.34 Å, and the distances for (NH)$_{ZIF-8}$-(OH)$_{PIM-1}$ and (NH)$_{ZIF-8}$-(CH$_3$)$_{PIM-1}$ were ~3.26 and 2.70 Å, respectively. The results verified that the ZIF-8/PIM-1 MMMs possessed excellent interfacial compatibility.

Cross-sectional scanning electron microscope (SEM) images of the pristine membrane and ZIF-8/PIM-1 MMMs with varying ZIF-8 contents are shown in Fig. 1. As observed in Fig. 1 *B–D*, the ZIF-8 particles were homogeneously embedded within the PIM-1 matrix. In addition to the small size of the in situ formed ZIF-8, the interactions between the uncoordinated imidazole groups of ZIF-8 and the nitrile groups in PIM-1 chains also played important roles in the formation of defect-free interfaces in MMMs (37). However, when the Zn^{2+} content exceeded 0.15 mmol, excessive ZIF-8 loading in the PIM-1 matrix led to the formation of evident nonselective defects (Fig. 1 *D* and *E*). This could be ascribed to the excessive ZIF-8
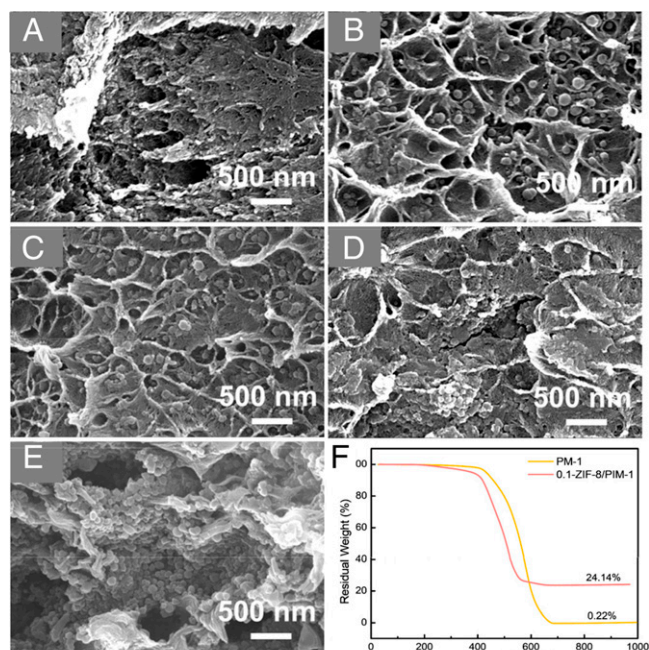
Fig. 1. SEM cross-sectional images of (*A*) PIM-1, (*B*) 0.05-ZIF-8/PIM-1, (*C*) 0.1-ZIF-8/PIM-1, (*D*) 0.15-ZIF-8/PIM-1, and (*E*) 0.2-ZIF-8/PIM-1 and (*F*) TGA curves of pure PIM-1 and 0.1-ZIF-8/PIM-1 at air atmosphere.

nanoparticles hindering PIM-1 chain packing. The wider view of 0.1-ZIF-8/PIM-1 also shows good dispersion of ZIF-8 nanoparticles in the membrane (*SI Appendix*, Fig. S6). The ZIF-8 content in the 0.1-ZIF-8/PIM-1 MMM was confirmed by thermal gravimetric analysis (TGA) under air atmosphere, as shown in Fig. 1*F*. The residual weights of PIM-1 and 0.1-ZIF-8/PIM-1 were 0.22 and 24.14%, respectively. The excess residual weight of 0.1-ZIF-8/PIM-1 was attributed to zinc oxide, and the

value represented an actual ZIF-8 loading in the membrane of up to 67.2 wt %, considering the chemical formula of ZIF-8 (i. e., $C_8H_{10}N_4Zn$).

The X-ray diffraction (XRD) patterns in Fig. 2*A* confirm the successful growth of ZIF-8 crystals in the MMMs. The main peaks of pure ZIF-8, referred to as (110), (200), (211), (220), (310), and (222) faces, were observed in all the MMMs patterns. Higher MOF loadings in PIM-1, that is, higher Zn^{2+} content, enhanced the peak intensities characteristic of ZIF-8 crystals. Compared to the peak positions of pristine ZIF-8 nanoparticles, the peak positions of ZIF-8 in our MMMs shifted toward higher 2θ angles. This suggests a contraction of the ZIF-8 lattice in our MMMs, which can be attributed to the distortion of the ZIF-8 framework caused by the affinity interactions between imidazole groups in the ZIF-8 and PIM-1 chains (38). Fourier transform infrared (FT-IR) spectra of the various MMMs studied here and ZIF-8 are shown in Fig. 2*B*. The spectrum of the pure PIM-1 membrane was identical to that reported in the literature (39), including the stretching vibrations of alkane C–H bonds (2,840, 2,930, and 2,950 cm^{-1}), nitrile groups (2,280 cm^{-1}), aromatic C–O (1,100 to 1,300 cm^{-1}), and the blending vibrations of aromatic C=C (1,600 cm^{-1}) and alkane C–H (1,450 cm^{-1}). No new peaks appeared in the spectrum of symbiosis-inspired synthesized MMMs, but the adsorption intensities for alkane C–H, nitrile groups, and aromatic C–O bonds decreased compared with those of the pure PIM-1 membrane. This indicates that no strong chemical interactions occurred between the ZIF-8 and PIM-1 chains. The increase in the relative peak intensity of Zn-N (421 cm^{-1}) is correlated with increasing ZIF-8 content. The TGA curves in Fig. 2*C* represent the thermogravimetric curves in N_2 atmosphere of neat PIM-1, MMMs, and ZIF-8. Pure PIM-1 showed good thermal stability up to ~400 °C due to the strong dipolar interactions among the nitrile groups of PIM-1 backbones (40). The growth of ZIF-8 nanoparticles in the PIM-1 matrix altered the thermal stability of the resultant MMMs. The mass loss at 400 °C for 0.05-ZIF-8/PIM-1 and 0.1-ZIF-8/PIM-1 decreased owing to the good thermal stability of ZIF-8. However, the

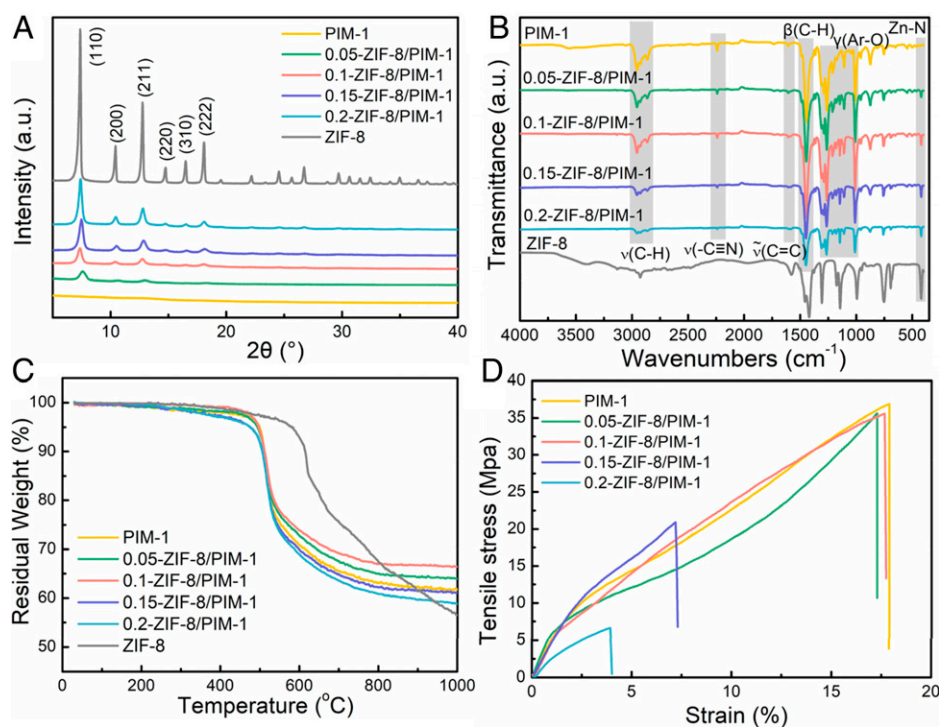**Fig. 2.** (*A*) XRD pattern, (*B*) FT-IR spectra, (*C*) TGA curves in N_2 atmosphere, and (*D*) tensile strength of membranes.

mass losses at 400 °C for 0.15-ZIF-8/PIM-1 and 0.2-ZIF-8/PIM-1 were higher than those of pure PIM-1, possibly because the excessive MOF content disrupted dipolar interactions between PIM-1 chains, leading to easier PIM-1 thermal decomposition (41). The residual weight of ZIF-8 at 1,000 °C was lower than that of PIM-1, but the residual weights for the 0.05-ZIF-8/PIM-1 and 0.1-ZIF-8/PIM-1 MMMs remained larger than those of ZIF-8 and PIM-1. This could be attributed to the formation of zinc oxides, where oxygen was produced during PIM-1 decomposition and bonds with Zn^{2+} in ZIF-8. At much higher ZIF-8 content, the large mass loss of ZIF-8 became the primary factor; therefore, the residual weights of the resulting MMMs were lower than that of PIM-1. The mechanical properties (elongation at break and tensile strength) of the ZIF-8/PIM-1 MMMs were characterized by elongation at break and tensile strength reduced when compared to PIM-1 (Fig. 2D). This is ascribed to the decrease in membrane ductility with ZIF-8 incorporation. However, the mechanical properties of the 0.05-ZIF-8/PIM-1 and 0.1-ZIF-8/PIM-1 MMMs were similar to those of PIM-1, indicating that optimal MOF loadings were crucial for good ZIF-8 dispersion, leading to excellent polymer–filler interfaces in symbiosis-inspired MMMs.

Gas Separation Performance. Pure gas permeabilities were tested, and the corresponding results are summarized in Fig. 3A and *SI Appendix*, Table S1, especially for CO_2 separation. The gas permeabilities of all MMMs studied decreased in the order of CO_2 (kinetic diameter of 3.3 Å) > H_2 (2.89 Å) > CH_4 (3.8 Å) > N_2 (3.64 Å). With increasing Zn^{2+} content up to 0.2 mmol (i.e., ZIF-8 loading), CO_2 and CH_4 permeability increased by 141 and 371%, respectively, and H_2 and N_2 permeability first decreased and then increased. CO_2/N_2 selectivity increased from 22.6 to 24.8, as Zn^{2+} content increased from 0 to 0.05 mmol and was reduced to 11.9 at Zn^{2+} content >0.1 mmol. Meanwhile, the CO_2/CH_4 selectivity of our MMMs was reduced from 17.6 to 15.8 (10.2% decrease) at 0.05 mmol Zn^{2+} content. As the Zn^{2+} content increased to 0.1 mmol, the CO_2/CH_4 selectivity reached a maximum value of 18.8. It is well known that gas transport through a membrane is underpinned by the solubility of gas molecules (related to the critical temperature of the gas molecules) as well as the gas diffusivity across the membrane (related to the kinetic diameter) (42). To explain the gas permeability and selectivity trends observed in our MMMs, we determined the diffusivity and solubility coefficients using the time lag method (Fig. 3 B and C). The incorporation of 0.05 mmol Zn^{2+} into PIM-1 via our symbiosis-inspired approach reduced CO_2 diffusivity when compared to pristine PIM-1. As the Zn^{2+} content reached 0.1 mmol, the CO_2 diffusivity increased from 0.816 to 1.704 cm^2/s, which is still lower than that of pristine PIM-1 (3.592 cm^2/s). However, N_2 and CH_4 diffusivities increased as the Zn^{2+} content increased from 0 to 0.1 mmol. All gas diffusivities were enhanced with ZIF-8 content >67.2 wt % (0.1 mmol Zn^{2+} content) as defects started to form and became nonselective. The maximum equivalent radii for the interfacial microvoids of PIM-1 was (6.3 ± 0.5) Å, and ZIF-8 possessed cavities with diameters of 11.6 Å that were accessible through flexible microporous windows of 3.4 Å (37). Considering the pore sizes of PIM-1 and ZIF-8, the incorporation of ZIF-8 cannot effectively enhance the gas diffusivity (*SI Appendix*, Table S2). This was validated by N_2 adsorption/desorption tests (using Beishide Instrument, BSD-PM), where the Brunauer-Emmett-Teller (BET) specific surface area, micropore volume, and pore size of 0.1-ZIF-8/PIM-1 were similar to those of the pure PIM-1 membrane (*SI Appendix*, Fig. S7). As both CO_2/N_2 and CO_2/CH_4 diffusivity selectivity decreased in ZIF-8 loaded MMMs, it was clear that ZIF-8 did not enhance size sieving. This could be due to the negligible size difference of CO_2, N_2, and CH_4 molecules and the flexible pore size of ZIF-8, which compromises the diffusivity selectivity.

The gas solubilities of the MMMs studied here increased by 358% for CO_2, 25.2% for N_2, and 10.0% for CH_4 as the Zn^{2+} content increased from 0 to 0.05 mmol. Further increments in ZIF-8 loading reduced the gas solubility of our symbiosis-inspired MMMs. The solubility trend of our MMMs contrasted with the gas diffusivity trends, especially for CO_2. This was primarily due to the selective adsorption of CO_2 by ZIF-8. The incorporation of ZIF-8 rigidified PIM-1 chains and reduced their flexibility, decreasing N_2 and CH_4 solubility, as shown in Fig. 3C. This also reduced CO_2 solubility when the Zn^{2+} content was up to 0.15 and 0.2 mmol. The CO_2/N_2 and CO_2/CH_4 solubility selectivities increased by 979 and 366%, respectively, as the ZIF-8 content increased from 0 to 0.1 mmol. These enhancements in CO_2/N_2 and CO_2/CH_4 solubility selectivities were enough to offset the reductions in CO_2/N_2 and CO_2/CH_4 diffusivity selectivities, underpinning the 7.96 and 6.81% improvements in CO_2/N_2 and CO_2/CH_4 separations, respectively. The relatively smaller increments in CO_2/CH_4 separation are ascribed to the condensability of CH_4 (43).

The results indicated that our symbiosis-inspired approach to incorporate ZIF-8 into PIM-1 resulted in solubility-selective MMMs. This contrasts with previous works on MMMs comprising polymer matrices composed of polyethylene oxide and polyimide, where MOFs increased the diffusivity selectivity of MMMs (34, 44, 45). In our work, the polymer matrix of PIM-1 was a super glassy polymer, with abundant interconnected micropores of maximum equivalent radii of 6.3 ± 0.5 Å. Additionally, the pore size of ZIF-8 was 46% smaller than that of PIM-1. Hence, the incorporation of ZIF-8 could not effectively enhance diffusivity selectivity. Moreover, most reported MOF/PIM-1 MMMs (33, 36, 38, 46, 47) contain low MOF loadings (< 20 wt %), i.e., a noncontinuous MOF phase or defective polymer-MOF interfaces. However, in our work, the simultaneous realization of high ZIF-8 content, excellent dispersion, and good interfacial compatibility achieved ultrahigh gas permeabilities and good gas selectivities of symbiosis-inspired MMMs by fully exploiting the unique characteristics of both MOFs and matrix.

The competing effects of adsorption and physical aging in both 0.1-ZIF-8/PIM-1 and pristine PIM-1 membranes were characterized by long-term stability tests up to 240 h under continuous gas (CO_2 or N_2) flow (Fig. 3D). During the initial 12 h, the CO_2 permeability of pristine PIM-1 membrane increased by 4.7%, from 3,939 to 4,125 barrer, which was attributed to the adsorption of CO_2 into PIM-1. From the 36th hour onward, the CO_2 permeability decreased due to the dominant effect of physical aging. The variation trend of CO_2/N_2 selectivity was consistent with that of CO_2 permeability. The losses in CO_2 permeability (i.e., 7.22%) and selectivity (i.e., 9.46%) for the 0.1-ZIF-8/PIM-1 were significantly smaller than those observed in pristine PIM-1, which indicated the significantly enhanced stability of 0.1-ZIF-8/PIM-1 membrane due to the compatible ZIF-8 rigidifying PIM-1 chains and hindering chain relaxation, thus mitigating physical aging (36, 38, 46). Moreover, the high MOF loadings effectively slowed down the physical aging rates of PIM-1, where the CO_2 permeability of 0.1-ZIF-8/PIM-1 membrane decreased by only 24% after 300-d natural aging (stored in ambient conditions), while the pristine PIM-1 benchmark showed a 44% drop in CO_2 permeability. Consequently, the CO_2/N_2 and CO_2/CH_4 selectivities of 0.1-ZIF-8/PIM-1 membrane increased by 4.5 and 12.8%, respectively, more gently when compared to 18.6 and 16.5% of PIM-1 (*SI Appendix*, Fig. S8). The effects of applied pressures on CO_2-induced plasticization behaviors of MMMs were explored and shown in *SI Appendix*, Fig. S9. The variation in CO_2 permeability was attributed to the CO_2 plasticization effect, which increased the free volume of the polymer (17). As a result, the CO_2/N_2 selectivity increased with feed pressures as the N_2
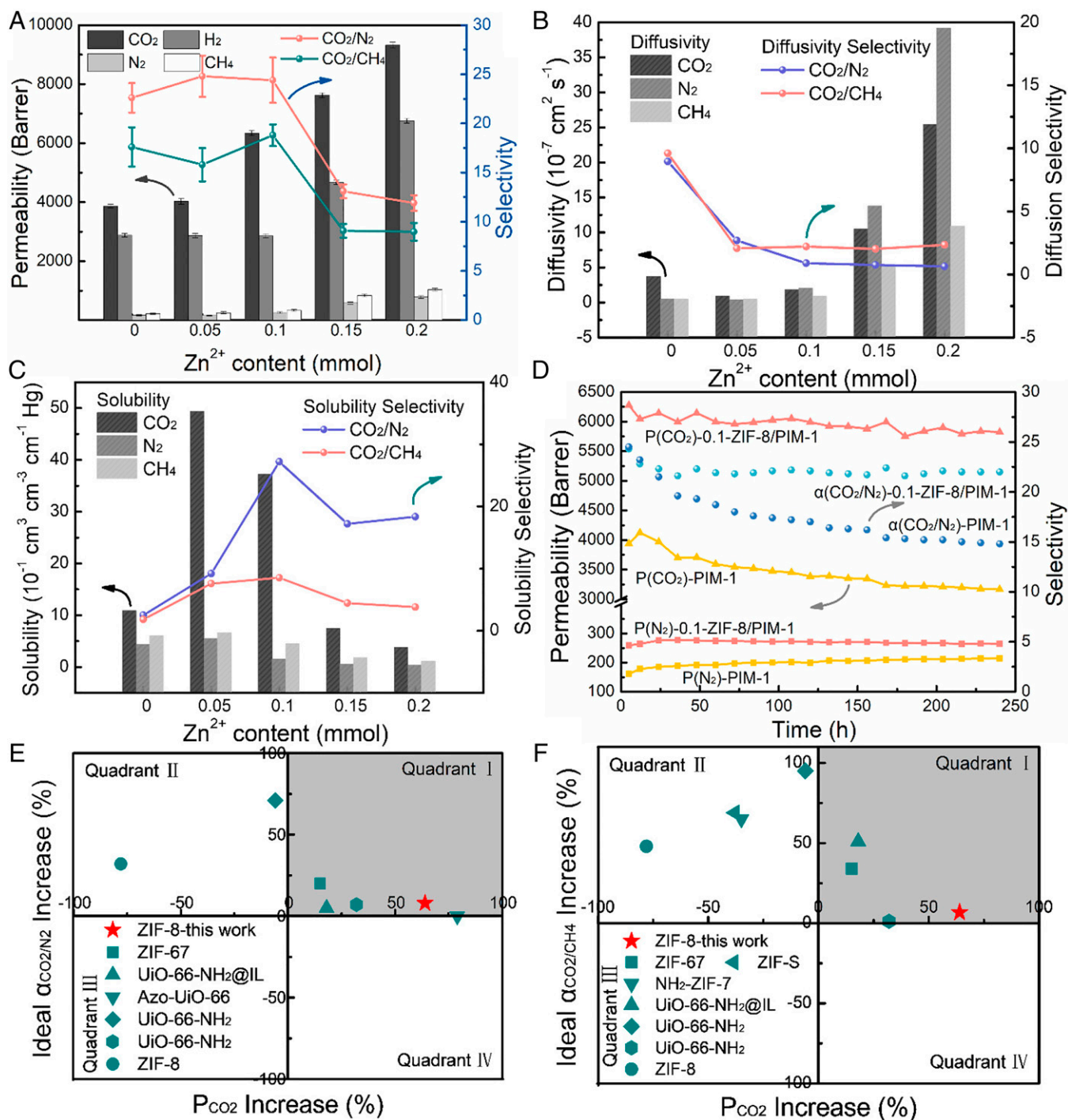
Fig. 3. (*A*) Permeability and selectivity, (*B*) diffusivity and diffusivity selectivity, (*C*) solubility and solubility selectivity, (*D*) long-term stability of membranes, and selectivity versus permeability increase of MOF/PIM-1 MMMs for (*E*) CO_2/N_2 and (*F*) CO_2/CH_4, where red stars represent 0.1-ZIF-8/PIM-1 in this work, and dark cyan shapes represent the data from references, as listed in *SI Appendix*, Table S3.

permeability slightly decreased. In comparison, the changes in CO_2 permeability and CO_2/N_2 selectivity for the 0.1-ZIF-8/PIM-1 membrane were smaller than those of the PIM-1 benchmark, which suggested that the incorporation of ZIF-8 suppressed CO_2 plasticization. The enhanced CO_2/N_2 selectivity validated the defect-free interface, considering that the presence of defects would greatly increase all gas permeabilities and decrease gas selectivities under higher pressures. In addition, the gas separation performances at different temperatures from 35 to 50 °C were evaluated. As shown in *SI Appendix*, Fig.

S10, the CO_2 permeabilities of PIM-1 and 0.1-ZIF-8/PIM-1 decreased by 58.7% and 44.6% from 35 to 50 °C, respectively, while the N_2 and CH_4 permeabilities increased. The decrease in CO_2 permeability was mainly due to the rapid drop in sorption at higher temperatures. As a result, the CO_2/N_2 and CO_2/CH_4 selectivities decreased with temperatures for both PIM-1 and 0.1-ZIF-8/PIM-1 membranes. Interestingly, the 0.1-ZIF-8/PIM-1 membrane always exhibited the better separation performance with both higher CO_2 permeability and CO_2 selectivities than pristine PIM-1 membrane in the temperature range from

He et al.
Symbiosis-inspired de novo synthesis of ultrahigh MOF growth mixed matrix
membranes for sustainable carbon capture

PNAS | 5 of 9
https://doi.org/10.1073/pnas.2114964119

35 to 50 °C. We also compared the CO_2/N_2 and CO_2/CH_4 separation performances of our symbiosis-inspired MMMs with MOF/PIM-1 MMMs reported in the literatures (Fig. 3 *E* and *F*). Quadrant I represented the most desirable improvements in both permeabilities and selectivities. Conventional ZIF-8/PIM-1 MMMs typically sacrificed CO_2 permeabilities to increase CO_2/N_2 and CO_2/CH_4 selectivities. Hence, the data of their CO_2/N_2 and CO_2/CH_4 separation performances were located in quadrant II. This is significantly different from the CO_2/N_2 and CO_2/CH_4 separation performances of our symbiosis-inspired MMMs, which can be found in quadrant I. This could be ascribed to the ultrahigh MOF loading, so that the CO_2 selective adsorption of MOF could be fully exploited. This was also key for the observed 64% improvement in CO_2 permeability, 8.0 and 6.8% improvement in CO_2/N_2 and CO_2/CH_4 selectivities, respectively. Furthermore, the CO_2 permeability increments in our symbiosis-inspired MMMs surpassed most of the MOF/PIM-1 MMMs. The incorporation of Azo-UiO-66 increased CO_2 permeability by 79% but had little influence on the CO_2/N_2 selectivity. Above all, our symbiosis-inspired method exhibited superiority to other works by overcoming the trade-off relationship between permeability and selectivity, i.e., increasing gas permeability with noticeable minor selectivity enhancements (*SI Appendix*, Table S3). Mixed-gas tests for CO_2/N_2 and CO_2/CH_4 were also carried out for PIM-1 and ZIF-8/PIM-1 MMM (*SI Appendix*, Table S4). With competitive sorption between CO_2 and N_2 or CH_4 in both PIM-1 and ZIF-8 nanopores, the CO_2 mixed gas permeabilities and selectivities of CO_2/N_2 and CO_2/CH_4 were lower than those obtained from pure gas tests for both pure PIM-1 and the synthesized MMM, which is consistent with the phenomena reported in other microporous polymer membranes (48).

To further clarify the effects of the symbiosis-inspired synthesis of ZIF-8 on the gas separation performance of the resultant MMMs, we used the first principle to perform all spin-polarization density functional theory calculations within the generalized gradient approximation using the Perdew–Burke–Ernzerhof formulation. The CO_2 adsorption processes in PIM-1

or ZIF-8 are illustrated in Fig. 4*A*, and the calculated CO_2 adsorption energies are shown in Fig. 4*B*. The absolute values of the adsorption energy of every adsorption site in ZIF-8 were higher than those of PIM-1, especially for the Zn site in ZIF-8, indicating the increased CO_2 affinity of ZIF-8 compared to PIM-1. Therefore, the incorporation of ZIF-8 in MMMs significantly enhanced the CO_2 solubility, which is consistent with our experimental findings based on the time lag method. CO_2 adsorption/desorption experiments of PIM-1 and 0.1-ZIF-8/PIM-1 were performed at 35 °C, corresponding to the gas permeation test conditions, and the results are shown in Fig. 4*C*. The CO_2 adsorption capacity of symbiosis-inspired MMM was 124 cm^3 g^{-1}, 13.8% higher than that of pure PIM-1, representing higher CO_2 solubility, according to Eqs. **1** and **2**. In addition, the CO_2/CH_4 solubility selectivities of PIM-1 were calculated based on the obtained CO_2 and CH_4 adsorption capacity (*SI Appendix*, Fig. S11). The CO_2/CH_4 solubility selectivity of the 0.1-ZIF-8/PIM-1 increased by 81% compared to that of the pure PIM-1 (i.e., 2.86 vs. 1.58), which is consistent with the results calculated via the time-lag method.

$$C = k_D p + \frac{C'_H b p}{1 + b p} , \qquad \textbf{[1]}$$

$$S = \frac{C}{p} = k_D + \frac{C'_H b}{1 + b p} , \qquad \textbf{[2]}$$

where C is the quantity adsorbed, cm^3 (STP) cm^{-3} (polymer). k_D refers to the Henry solubility coefficient, cm^3 (STP) cm^{-3} (polymer) cm Hg^{-1}. C'_H represents the Langmuir saturation constant, cm^3 (STP) cm^{-3} (polymer). b and p are the Langmuir affinity constant and pressure, respectively. S is the solubility coefficient of the gas in the membranes.

Superiority of Our Symbiosis-Inspired Method. To clearly illustrate the superiority of our symbiosis-inspired method for MMM fabrication, we compared the gas separation performances of our MMMs with those produced from traditional mixing methods such as physical blending (named as TM-67.2 wt %-ZIF-8/PIM-1). However, for TM-67.2 wt %-ZIF-8/PIM-1, the weak
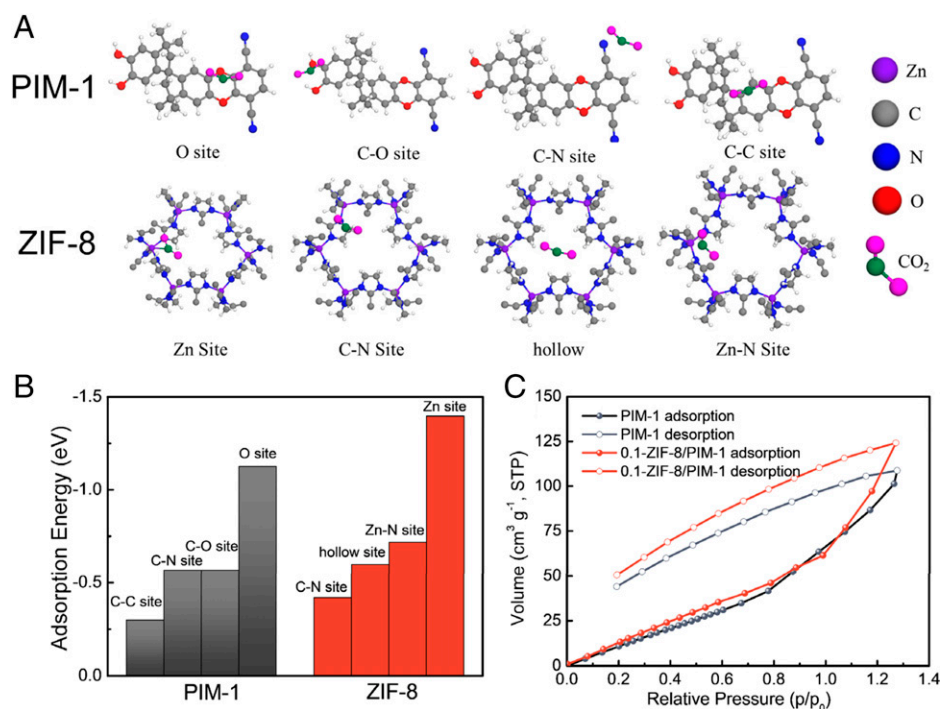

Fig. 4. (*A*) Adsorption structure of CO_2 within PIM-1 and ZIF-8, (*B*) CO_2 adsorption energy, and (*C*) CO_2 adsorption/desorption isotherm at 308 K.

load transfer between the polymer matrix and ZIF-8 nanoparticles made it difficult to form a piece of membrane containing 67.2 wt % of ZIF-8 (*SI Appendix*, Fig. S12C), and notable cracks/defects were observed in the cross-sections of MMMs with such high ZIF-8 loading (*SI Appendix*, Fig. S12F). The conceivable gas separation mechanisms of the traditional and symbiosis-inspired ZIF-8/PIM-1 MMMs are shown in Fig. 5 *A* and *B*. The traditional mixing method limited the ZIF-8 corporation content, which might induce agglomeration and form nonselective defects. Therefore, significant increases in gas permeability are mirrored by considerable gas selectivity losses. In contrast, our symbiosis-inspired strategy formed nanoparticles of ZIF-8 in situ polymer mixing, which intertwined with the polymer matrix. This was also critical to realize up to 67.2 wt % ZIF-8 content in MMMs that consequently enhanced adsorption effectively. The combination of enhanced CO_2 solubility and interfacial compatibility underpinned the concomitant enhancement of gas permeability and selectivity in our symbiosis-inspired MMMs.

In addition, we demonstrated the universality of our approach with different MOFs (ZIF-7 and ZIF-67) that could be fabricated in aqueous solutions at room temperature. As *SI Appendix*, Fig. S13 *A and B* show, ZIF-67 and ZIF-7 could be in situ synthesized successfully in PIM-1 matrix. The MOF content in these MMMs was even higher than that of ZIF-8/PIM-1 MMMs, and the ZIF-7 and ZIF-67 content reached 71.9 and 82.5 wt %, respectively (*SI Appendix*, Fig. S14A). These MMMs also demonstrated good gas separation performance (Fig. 5 *C* and *D*). Due to the smaller pore size of ZIF-7 (2.4 Å) and ZIF-67 (<3.4 Å), 0.1-ZIF-7/PIM-1 exhibited excellent H_2/N_2 selectivity of 19.3, and 0.1-ZIF-67/PIM-1 showed outstanding H_2/N_2 (24.5) and CO_2/N_2 (34.5) selectivities. The gas separation performance of the ZIF-67– and ZIF-7–based MMMs could be further improved after optimization because the smaller pore size could play an important role in size sieving ability. The different pore sizes of ZIFs endowed the ability to separate different gases, which may broaden the application
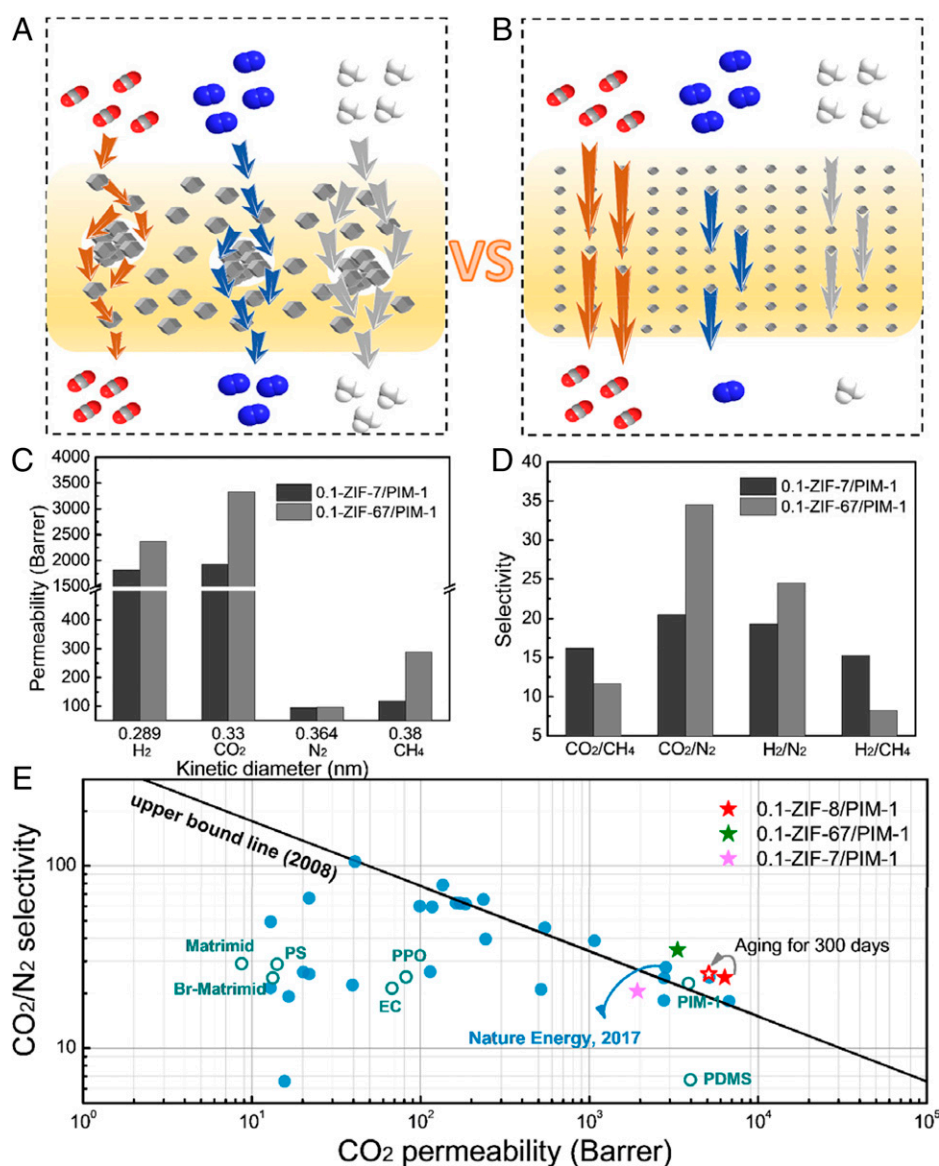
Fig. 5. Gas transmission schematic of MMMs with high MOF loading via (*A*) traditional mixing method and (*B*) our symbiosis-inspired method, (*C*) permeability, (*D*) selectivity of 0.1-ZIF-7/PIM-1 and 0.1-ZIF-67/PIM-1, and (*E*) selectivity versus permeability for CO_2/N_2, where gas separation performance of the MMMs prepared in this work (stars), primary common polymeric membranes (hollow circles), and various MOF-based MMMs from literature (solid circles) are plotted against the Robeson plot of 2008 (13). A fully detailed comparison of the data in this plot is in *SI Appendix*, Table S6.

He et al.
Symbiosis-inspired de novo synthesis of ultrahigh MOF growth mixed matrix membranes for sustainable carbon capture

PNAS | 7 of 9
https://doi.org/10.1073/pnas.2114964119

fields. As Fig. 5*E* and *SI Appendix*, Fig. S15 illustrate, the gas separation performances of all MMMs studied here surpassed those of most MOF-based MMMs. The CO_2/N_2 separation performances of the 0.1-ZIF-8/PIM-1 and 0.1-ZIF-67/PIM-1 MMMs were beyond the 2008 upper bound line (13). We also exploited this strategy to fabricate MMMs with another polymer matrix, Matrimid, a commercially available polyimide (*SI Appendix*, Table S7). With up to 61.7 wt % ZIF-8 loading (*SI Appendix*, Fig. S14*B*), the CO_2 permeability of Matrimid increased by 331%, and H_2 permeability increased by 285% with only slightly sacrificed gas selectivity. The effects of our symbiosis-inspired approach for MOF incorporation in polymer matrices were better demonstrated with Matrimid. This is because as MOFs become the continuous phase in a polymer with better-packed chains, an excess gas path is created in a low-permeability matrix, enhancing gas transport.

Conclusions

We developed a de novo strategy to construct MMMs with ultrahigh ZIF-8 content, inspired by the process of a rhizobium-inducing nodule for integrated symbiosis. With the help of the $CHCl_3$/water mixture, the ZIF-8 crystals became smaller (~100 nm) and uniformly dispersed in the highly permeable PIM-1 matrix simultaneously, which can accommodate massive MOF loadings of up to unparalleled 67.2 wt %, significantly beneficial to gas transportation in MMMs. Notably, the CN group of PIM-1 interacted with the NH group of ZIF-8, resulting in excellent interfacial compatibility, which prevented nonselective defects under such ultrahigh MOF content without agglomeration. The ultrahigh MOF incorporation effectively promotes the gas solubility in symbiosis-inspired MMMs, which is significantly different from the role of the relatively low-content MOF in other polymeric matrices. The optimized membrane exhibited a superior CO_2 permeability of 6,338 barrer, while maintaining good selectivity for energetic-efficient carbon capture. The ultrahigh MOF incorporation alleviates the PIM-1's physical aging and plasticization of, and maintains the long-term stability of, the synthesized MMMs. Our proposed symbiosis-inspired approach could overcome long-standing issues associated with the perfect combination and fully exploiting the inherent merits of two well-known materials, providing a universal toolbox for constructing next-generation high-performance MMMs with diverse MOFs and various polymer matrices for sustainable gas separation, which also open the mind to fabricate MOF-based composite materials.

Materials and Methods

Synthesis of PIM-1. First, 3.41 g (10 mmol) 5,5′,6,6′-tetrahydroxy-3,3,3′,3′-tetramethyl-1,1′-spirobisindane (TTSBI) and 2.01 g (10 mmol) 2,3,5,6-tetrafluoro-terephthalonitrile (TFTPN) were dissolved in 30 mL DMF and then added to 150 mL cyclohexane. The mixture was stirred at 60 °C for 72 h under N_2 atmosphere. It was poured into methanol to obtain flocculent precipitate after cooling to room temperature and then filtered to obtain a yellow solid. The resultant polymer was dissolved in $CHCl_3$ and reprecipitated from MeOH three times for purification and then dried under vacuum at 80 °C for 12 h. Pure products were collected for further usage.

Fabrication of ZIF-8/PIM-1 MMMs via In Situ Growth Method. First, 0.1 g pure PIM-1 was dissolved in 10 g $CHCl_3$ with stirring for 5 h to form homogeneous solution. Then, 1 mL aqueous solution containing a certain content (0.05, 0.1, 0.15, 0.2, and 0.25 mmol) of $Zn(NO_3)_2 \cdot 6H_2O$ was added into PIM-1 solution with continuous stirring. After mixing fully for 30 min, 4 mL Hmim aqueous solution containing a 60-fold Zn^{2+} amount was poured inside and was continuously and vigorously stirred for 6 h. Then, the whole mixture was poured into excess MeOH to precipitate PIM-1 and ZIF-8 simultaneously, forming a uniform ZIF-8/PIM-1 mixture. After washing with MeOH, filtering, and drying, ZIF-8@PIM-1 was dissolved in 10 g $CHCl_3$ and then cast in a mold. The obtained membranes after solvent evaporation were soaked in MeOH for 24 h to activate ZIF-8 and swell PIM-1 simultaneously and then dried at 80 °C overnight. The membranes were named as x-ZIF-8/PIM-1, where x referred to the amount of Zn^{2+} with the unit mmol.

Data Availability. All study data are included in the article and/or *SI Appendix*.

1. R. J. Millar *et al.*, Emission budgets and pathways consistent with limiting warming to 1.5 °C. *Nat. Geosci.* **10**, 741–747 (2017).
2. X. Jiang, S. Li, L. Shao, Pushing CO_2-philic membrane performance to the limit by designing semi-interpenetrating networks (SIPN) for sustainable CO_2 separations. *Energy Environ. Sci.* **10**, 1339–1344 (2017).
3. S. Li, X. Jiang, X. Yang, Y. Bai, L. Shao, Nanoporous framework "reservoir" maximizing low-molecular-weight enhancer impregnation into CO_2-philic membranes for highly-efficient CO_2 capture. *J. Membr. Sci.* **570-571**, 278–285 (2019).
4. C. Hepburn *et al.*, The technological and economic prospects for CO_2 utilization and removal. *Nature* **575**, 87–97 (2019).
5. L. Rosa, D. L. Sanchez, M. Mazzotti, Assessment of carbon dioxide removal potential via BECCS in a carbon-neutral Europe. *Energy Environ. Sci.* **14**, 3086–3097 (2021).
6. R. W. Baker, K. Lokhandwala, Natural gas processing with membranes: An overview. *Ind. Eng. Chem. Res.* **47**, 2109–2121 (2008).
7. M. Carta *et al.*, An efficient polymer molecular sieve for membrane gas separations. *Science* **339**, 303–307 (2013).
8. J. Liu *et al.*, Highly polar but amorphous polymers with robust membrane CO_2/N_2 separation performance. *Joule* **3**, 1881–1894 (2019).
9. P. M. Budd *et al.*, Polymers of intrinsic microporosity (PIMs): Robust, solution-processable, organic nanoporous materials. *Chem. Commun. (Camb.)* **2**, 230–231 (2004).
10. P. M. Budd *et al.*, Solution-processed, organophilic membrane derived from a polymer of intrinsic microporosity. *Adv. Mater.* **16**, 456–459 (2004).
11. P. Budd *et al.*, Gas separation membranes from polymers of intrinsic microporosity. *J. Membr. Sci.* **251**, 263–269 (2005).
12. P. Li, T. S. Chung, D. R. Paul, Gas sorption and permeation in PIM-1. *J. Membr. Sci.* **432**, 50–57 (2013).
13. L. M. Robeson, The upper bound revisited. *J. Membr. Sci.* **320**, 390–400 (2008).
14. R. W. Baker, B. T. Low, Gas separation membrane materials: A perspective. *Macromolecules* **47**, 6999–7013 (2014).
15. M. Z. Ahmad, R. Castro-Muñoz, P. M. Budd, Boosting gas separation performance and suppressing the physical aging of polymers of intrinsic microporosity (PIM-1) by nanomaterial blending. *Nanoscale* **12**, 23333–23370 (2020).
16. M. Heuchel, D. Fritsch, P. M. Budd, N. B. McKeown, D. Hofmann, Atomistic packing model and free volume distribution of a polymer with intrinsic microporosity (PIM-1). *J. Membr. Sci.* **318**, 84–99 (2008).
17. R. R. Tiwari, J. Jin, B. D. Freeman, D. R. Paul, Physical aging, CO_2 sorption and plasticization in thin films of polymer with intrinsic microporosity (PIM-1). *J. Membr. Sci.* **537**, 362–371 (2017).
18. R. Swaidan, B. S. Ghanem, E. Litwiller, I. Pinnau, Pure- and mixed-gas CO_2/CH_4 separation properties of PIM-1 and an amidoxime-functionalized PIM-1. *J. Membr. Sci.* **457**, 95–102 (2014).
19. R. Hou *et al.*, Solvation effects on the permeation and aging performance of PIM-1-based MMMs for gas separation. *ACS Appl. Mater. Interfaces* **11**, 6502–6511 (2019).
20. K. Golzar, H. Modarress, S. Amjad-Iranagh, Effect of pristine and functionalized single- and multi-walled carbon nanotubes on CO_2 separation of mixed matrix membranes based on polymers of intrinsic microporosity (PIM-1): A molecular dynamics simulation study. *J. Mol. Model.* **23**, 266 (2017).
21. A. Gonciaruk, K. Althumayri, W. J. Harrison, P. M. Budd, F. R. Siperstein, PIM-1/graphene composite: A combined experimental and molecular simulation study. *Microporous Mesoporous Mater.* **209**, 126–134 (2015).
22. M. Chen *et al.*, Graphene oxide nanosheets to improve permeability and selectivity of PIM-1 membrane for carbon dioxide separation. *J. Ind. Eng. Chem.* **63**, 296–302 (2018).
23. T. Mitra, R. S. Bhavsar, D. J. Adams, P. M. Budd, A. I. Cooper, PIM-1 mixed matrix membranes for gas separations using cost-effective hypercrosslinked nanoparticle fillers. *Chem. Commun. (Camb.)* **52**, 5581–5584 (2016).
24. Y. Liu *et al.*, Single-crystalline ultrathin 2D porous nanosheets of chiral metal-organic frameworks. *J. Am. Chem. Soc.* **143**, 3509–3518 (2021).
25. G. Yu *et al.*, Constructing connected paths between UiO-66 and PIM-1 to improve membrane CO_2 separation with crystal-like gas selectivity. *Adv. Mater.* **31**, e1806853 (2019).
26. N. Tien-Binh, D. Rodrigue, S. Kaliaguine, In-situ cross interface linking of PIM-1 polymer and UiO-66-NH_2 for outstanding gas separation and physical aging control. *J. Membr. Sci.* **548**, 429–438 (2018).

8 of 9 | PNAS
https://doi.org/10.1073/pnas.2114964119

He et al.
Symbiosis-inspired de novo synthesis of ultrahigh MOF growth mixed matrix membranes for sustainable carbon capture

27. M. R. Khdhayyer et al., Mixed matrix membranes based on UiO-66 MOFs in the polymer of intrinsic microporosity PIM-1. *Separ. Purif. Tech.* **173**, 304–313 (2017).

28. H. Zhang et al., Ultrafast selective transport of alkali metal ions in metal organic frameworks with subnanometer pores. *Sci. Adv.* **4**, eaaq0066 (2018).

29. L. Ma, F. Svec, Y. Lv, T. Tan, Engineering of the filler/polymer interface in metal-organic framework-based mixed-matrix membranes to enhance gas separation. *Chem. Asian J.* **14**, 3502–3514 (2019).

30. J. Zhao et al., Manipulation of interactions at membrane interfaces for energy and environmental applications. *Prog. Polym. Sci.* **80**, 125–152 (2018).

31. R. Lin, B. Villacorta Hernandez, L. Ge, Z. Zhu, Metal organic framework based mixed matrix membranes: An overview on filler/polymer interfaces. *J. Mater. Chem. A Mater. Energy Sustain.* **6**, 293–312 (2018).

32. W. Wu, P. Su, W. Li, Mixed matrix membranes containing polymer-embedded metal-organic framework microspheres. *AIChE J.* **66**, e17028 (2020).

33. Y. Wang et al., Amino-functionalized ZIF-7 embedded polymers of intrinsic microporosity membrane with enhanced selectivity for biogas upgrading. *J. Membr. Sci.* **602**, 117970 (2020).

34. C. Ma, J. J. Urban, Hydrogen-bonded polyimide/metal-organic framework hybrid membranes for ultrafast separations of multiple gas pairs. *Adv. Funct. Mater.* **29**, 1903243 (2019).

35. X. Jiang et al., Aqueous one-step modulation for synthesizing monodispersed ZIF-8 nanocrystals for mixed-matrix membrane. *ACS Appl. Mater. Interfaces* **13**, 11296–11305 (2021).

36. C. Ye et al., Incorporating nano-sized ZIF-67 to enhance selectivity of polymers of intrinsic microporosity membranes for biogas upgrading. *Chem. Eng. Sci.* **216**, 115497 (2020).

37. M. Benzaqui et al., Toward an understanding of the microstructure and interfacial properties of PIMs/ZIF-8 mixed matrix membranes. *ACS Appl. Mater. Interfaces* **8**, 27311–27321 (2016).

38. X. Wu et al., Nanoporous ZIF-67 embedded polymers of intrinsic microporosity membranes with enhanced gas separation performance. *J. Membr. Sci.* **548**, 309–318 (2018).

39. N. Du et al., Polymer nanosieve membranes for CO_2-capture applications. *Nat. Mater.* **10**, 372–375 (2011).

40. N. Du et al., Polymers of intrinsic microporosity containing trifluoromethyl and phenylsulfone groups as materials for membrane gas separation. *Macromolecules* **41**, 9656–9662 (2008).

41. S. He et al., Intermediate thermal manipulation of polymers of intrinsic microporous (PIMs) membranes for gas separations. *AIChE J.* **66**, e16543 (2020).

42. L. M. Robeson, Correlation of separation factor versus permeability for polymeric membranes. *J. Membr. Sci.* **62**, 165–185 (1991).

43. L. Zhang, G. Wu, J. Jiang, Adsorption and diffusion of CO_2 and CH_4 in zeolitic imidazolate framework-8: Effect of structural flexibility. *J. Phys. Chem. C* **118**, 8788–8794 (2014).

44. X. Jiang, S. Li, S. He, Y. Bai, L. Shao, Interface manipulation of CO_2–philic composite membranes containing designed UiO-66 derivatives towards highly efficient CO_2 capture. *J. Mater. Chem. A Mater. Energy Sustain.* **6**, 15064–15073 (2018).

45. N. Tien-Binh, H. Vinh-Thang, X. Y. Chen, D. Rodrigue, S. Kaliaguine, Polymer functionalization to enhance interface quality of mixed matrix membranes for high CO_2/CH_4 gas separation. *J. Mater. Chem. A Mater. Energy Sustain.* **3**, 15202–15213 (2015).

46. M. Liu et al., High-throughput CO_2 capture using PIM-1@MOF based thin film composite membranes. *Chem. Eng. J.* **396**, 125328 (2020).

47. H. Yin, A. Alkaş, Y. Zhang, Y. Zhang, S. G. Telfer, Mixed matrix membranes (MMMs) using an emerging metal-organic framework (MUF-15) for CO_2 separation. *J. Membr. Sci.* **609**, 118245 (2020).

48. H. B. Park et al., Polymers with cavities tuned for fast selective transport of small molecules and ions. *Science* **318**, 254–258 (2007).

ENGINEERING

He et al.
Symbiosis-inspired de novo synthesis of ultrahigh MOF growth mixed matrix membranes for sustainable carbon capture

PNAS | 9 of 9
https://doi.org/10.1073/pnas.2114964119